Radiation-Induced Radicals in Glucose-1-phosphate. I. Electron Paramagnetic Resonance and Electron Nuclear Double Resonance Analysis of *in situ* X-Irradiated Single Crystals at 77 K

Hendrik De Cooman,[†,‡] Gauthier Vanhaelewyn,[†] Ewald Pauwels,[‡] Einar Sagstuen,[§] Michel Waroquier,[‡] and Freddy Callens*[,†]

Department of Solid State Sciences, Ghent University, Krijgslaan 281-S1, B-9000 Gent, Belgium, Center for Molecular Modeling, Ghent University, Proeftuinstraat 86, B-9000 Gent, Belgium, and Department of Physics, University of Oslo, P.O. Box 1048 Blindern, N-0316 Oslo, Norway

Received: May 14, 2008; Revised Manuscript Received: June 26, 2008

Electron magnetic resonance analysis of radiation-induced defects in dipotassium glucose-1-phosphate dihydrate single crystals *in situ* X-irradiated and measured at 77 K shows that at least seven different carbon-centered radical species are trapped. Four of these (R1−R4) can be fully or partly characterized in terms of proton hyperfine coupling tensors. The dominant radical (R2) is identified as a C1-centered species, assumedly formed by a scission of the sugar−phosphate junction and the concerted formation of a carbonyl group at the neighboring C2 carbon. This structure is chemically identical to a radical recently identified in irradiated sucrose single crystals. Radical species R1 and R4 most likely are C3- and C6-centered species, respectively, both formed by a net hydrogen abstraction. R3 is suggested to be chemically similar to but geometrically different from R4. Knowledge of the identity of the sugar radicals present at 77 K provides a first step in elucidating the formation mechanism of the phosphoryl radicals previously detected after X-irradiation at 280 K. In paper II, the chemical identity, precise conformation, and possible formation mechanisms of these radical species are investigated by means of DFT calculations and elementary insight into the radiation chemistry of sugar and sugar derivatives is obtained.

1. Introduction

Exposure of DNA to ionizing radiation initiates sequences of processes that eventually lead to various end points, among other single and double strand breaks. The primary precursors are free radicals formed in the base and the sugar−phosphate residues. Strand breaks appear to be induced primarily by damage to the sugar−phosphate groups, as indicated by a correlation between the yield of radiation-induced free radicals localized at the sugar and the yield of single strand breaks (ssb's) in irradiated DNA.[1,2] Sugar radicals may act as immediate precursors for the release of a phosphate group by an elimination process, as is well-known from aqueous radiation chemistry.[3] Both carbon-centered and phosphoryl radicals may be envisioned by such processes.

Recently, it has been suggested that low-energy electrons (LEE's) with energies below the ionization threshold may provoke direct damage to DNA through dissociative electron attachment (DEA), causing prompt cleavage of the sugar−phosphate ester bond.[4−6] Even if the number of LEE's is large, the number of radicals associated with this process is small.[2] It has also been suggested that excited base cation-radical states can lead to free radical damage to the sugar−phosphate backbone.[2,7]

Experimentally investigating radical processes leading to strand breaks, being initiated by direct radiation effects, necessitates the study of model systems containing the sugar−phosphate ester bond. A number of hydroxyalkyl phosphate derivatives have been studied by electron paramagnetic resonance (EPR) techniques in the solid state.[8−14] Hydroxyalkyl radicals are the major products formed subsequent to low-temperature irradiation. These may be formed by reductive processes initiated either by trapped electrons[15] or by DEA, by oxidative processes[16] or by elimination processes (direct H-atom abstraction). Phosphate radicals have been detected only in a few cases after 77 K irradiation[8,13] and not at all at very low temperatures (<77 K), so that, although prompt phosphate−ester bond breaks have been proposed to occur in irradiated DNA systems,[17] there is no direct evidence for these processes taking place in hydroxyalkyl phosphate derivatives. However, carbon-centered radicals are commonly formed. Several of these may have been formed by inorganic phosphate elimination possibly immediately following DEA, as the inorganic phosphate species is EPR silent.

SCHEME 1: Chemical Structure of a Glucose-1-phosphate Molecule

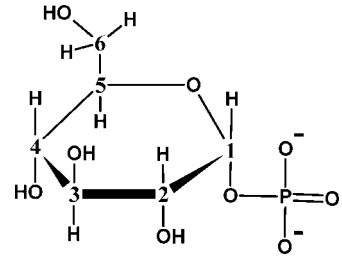

Glucose-1-phosphate (Scheme 1) is one such system where previous studies have demonstrated the formation of phosphate radicals at room temperature, implying processes involving the

* To whom all correspondence should be addressed. Phone: +3292644352. Fax: +32926464996. E-mail: freddy.callens@ugent.be.
† Department of Solid State Sciences, Ghent University.
‡ Center for Molecular Modeling, Ghent University.
§ Department of Physics, University of Oslo.

10.1021/jp804290e CCC: $40.75 © 2008 American Chemical Society
Published on Web 10/31/2008

phosphate−ester bond. From V-band (70 GHz) EPR and electron nuclear double resonance (ENDOR) measurements on crystals of the dipotassium salt of glucose-1-phosphate dihydrate (abbreviated K2G1P in this work) at 4.2 K after *in situ* X-irradiation at this temperature, Locher and Box[12] characterized three alkoxy radicals, one of which was identified as the O6-centered species. In addition, these authors identified an intermolecularly trapped electron and a C6-centered hydroxyalkyl radical. As detailed crystal data were not available for these authors, no further analysis could be made. However, the bulk of the absorption was reported to occur in the free spin region ($g \approx 2$) where the EPR signal is strongly composite, indicating that a major part of the radicals present at this temperature are carbon-centered. No evidence for phosphate radicals was observed.

Bungum and co-workers studied K2G1P single crystals X-irradiated at 280 K using X- and Q-band (9.5 and 34 GHz, respectively) EPR techniques at RT.[14] These authors observed two varieties of the phosphoryl radical ($^{\bullet}PO_3^{2-}$). Furthermore, reanalysis of the data of Locher and Box[12] and comparison with the crystal structure[18,19] by Bungum and co-workers confirm the identity of both the O6-centered alkoxy radical and the C6-centered hydroxyalkyl radical (H6b abstraction) and suggest that the other two alkoxy radicals are the O2- and O4-centered species.[20]

Nelson and co-workers performed measurements on irradiated frozen aqueous solutions of monosodium D-glucose-6-phosphate[21,22] which revealed that after X-irradiation at 77 K phosphoranyl radicals are formed. These species decay into two new different centers upon annealing to RT. One of these centers most likely is a phosphoryl radical, whereas no definite conclusion was arrived at with regard to the identity of the second one. For the composite central part of the spectrum arising from carbon-centered sugar radicals that also transform upon annealing, only very tentative attributions were made in terms of radical models.

A more elaborate and general study on phosphate radicals was published in 1996 by Sanderud and Sagstuen.[13] From powder EPR studies on several phosphate esters at both 77 and 275 K after *in situ* irradiation at these temperatures, these authors tentatively concluded that phosphoryl radicals may be formed through several distinct pathways, depending on the net charge and the protonation state of the parent phosphate group with hydroxyalkyl sugar radicals acting as precursors in each pathway suggested. In the case of K2G1P, no phosphoryl or phosphoranyl radicals were detected after irradiation at 77 K, but two varieties of phosphoryl radicals were observed at 275 K, in agreement with the results reported by Bungum and co-workers.[14] It was suggested that a sugar radical acts as a precursor for these phosphate radicals.

Thus, an interesting question arises for K2G1P: which initially formed species at low temperature transforms into the phosphate radicals detected at RT, and how? The prerequisite to answer this question is knowledge of the chemical identity of the sugar radicals present after 77 K X-irradiation. In the current work (this paper and the accompanying paper (paper II, ref 23)), the composite EPR signal at $g \approx 2$ of K2G1P single crystals irradiated and measured at 77 K was analyzed using experimental EPR techniques as well as computational density functional theory (DFT) calculations.

2. Experimental Procedures and Methods

Beevers and Maconochie[18] and later Narendra and Viswamitra[19] determined the crystal structure of K2G1P from X-ray diffraction studies. The latter study was considerably more accurate but included neither the hydroxy hydrogen atoms nor the water hydrogen atoms. Sugawara and Iwasaki[24] refined the data from Beevers and Maconochie,[18] thus providing the most accurate and complete set of atomic coordinates. The data of that study were used in the present work. The crystal is monoclinic with space group $P2_1$ and unit cell parameters $a = 10.458$ Å, $b = 9.027$ Å, $c = 7.532$ Å, and $\beta = 110.39°$. The atomic coordinates in the $\langle a^*bc \rangle$ frame of ref 24 are given in Supporting Information Table S1. A unit cell contains two glucose-1-phosphate molecules (each of them with a double negative charge on the phosphate group), four K^+ ions, and four water molecules. The chemical structure of a glucose-1-phosphate molecule is depicted in Scheme 1, together with the IUPAC-based numbering used for the carbon atoms. Hydrogens and oxygens are numbered in this work according to the carbon to which they are bound. Hydroxy hydrogens are indicated as HO*X*, with *X* being the number of the carbon to which the hydroxy group is bound. The ring oxygen is labeled as O5.

K2G1P single crystals were grown from saturated H_2O or D_2O solutions at RT. Crystallization of deuterated crystals from D_2O was successful, but recrystallization of these deuterated crystals from D_2O was not. This implies that, making a conservative estimate, a deuteration rate of 90% may be expected. The samples were oriented using Weissenberg X-ray diffraction techniques with the rotation axes parallel to a given axis and subsequently transferred to copper sample holders with minimal loss of alignment. Although an accuracy of 1° in principle is attainable with this method, samples could often be oriented to only a few degrees of accuracy due to the rather strong absorption of the X-rays. The samples were irradiated *in situ* at 77 K for up to 12 h using a Philips chromium target X-ray tube operated at 60 kV and 40 mA, resulting in a total dose up to 110 kGy. The spectrometer and measurement procedures were as described elsewhere.[25]

EPR and ENDOR angular variation measurements were performed in the three planes perpendicular to the $\langle a \rangle$, $\langle b \rangle$, and $\langle c \rangle$ axes in 5° intervals. At each orientation, ENDOR measurements were performed for at least two, and usually three or more, different magnetic field positions. An extensive number of ENDOR-induced EPR (EIE) measurements were carried out at several orientations in the three planes. The program MAGRES[26,27] was used to derive the proton hyperfine coupling tensors from the ENDOR data as previously described in, e.g., ref 28.

The simulations of the EPR and EIE spectra were carried out using Easyspin[29] subroutines in Matlab. Linewidths and *g* values were treated as variables for the fitting process. For the EIE angular variation simulations, an isotropic *g* value is assumed.

Whenever a comparison is made between calculated eigenvector directions and experimentally determined eigenvector directions or crystal directions, allowed symmetry operations ($b \rightarrow -b$ and inversion of eigenvectors) are performed to obtain the best possible agreement.

Throughout this work, the different radical species that are experimentally detected are labeled as R*x*, with *x* being a number from 1 to 7. For radical species R1 to R4, plausible model structures are put forward. These are labeled M*x* ($x = 1-4$) to emphasize the fact that these structures are "proposals", and not necessarily the actual structures. When there are two model structures for radical R*x*, they are labeled M*x*a and M*x*b.

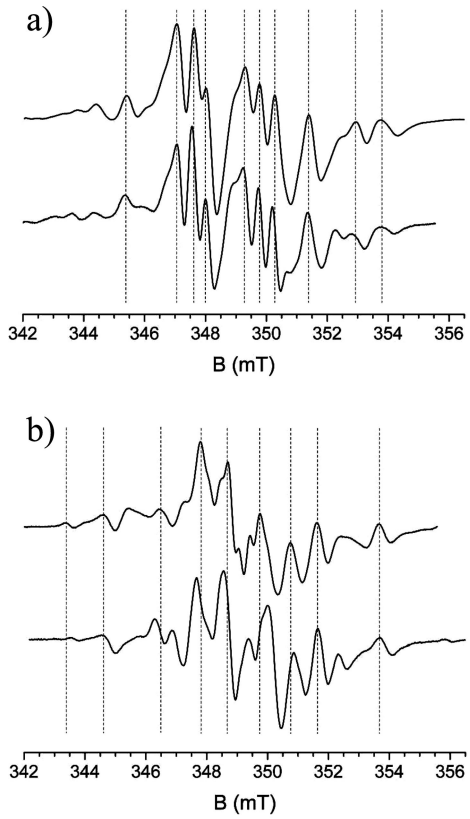

Figure 1. (a) EPR spectra obtained from measurements at 77 K after *in situ* X-irradiation at 77 K on K2G1P single crystals grown from an H_2O solution (top) and a D_2O solution (bottom). The magnetic field was perpendicular to $\langle b \rangle$, approximately 30° from $\langle a \rangle$, and 40° from $\langle c \rangle$. All spectra were normalized to a microwave frequency of 9.7750 GHz. (b) Same as part a but with the magnetic field approximately parallel to $\langle c^* \rangle$.

3. Results

Figure 1 shows EPR spectra for two different orientations of the crystal in the magnetic field, obtained from measurements on crystals grown from H_2O or D_2O solutions. Taking into account that orientations may differ up to 3° for the "H_2O spectrum" and the "D_2O spectrum", the similarity of the spectra suggests that the major radical species present in nondeuterated and deuterated samples are essentially the same and that none of the major hyperfine interactions is due to exchangeable protons. Angular variations of the EPR spectrum reveal only small anisotropies of the *g* tensors, indicating that all radicals with appreciable signal intensity are carbon-centered. Some more anisotropic, but very faint features, possibly due to an alkoxy radical, were observed, but these were not studied further.

The ENDOR spectra revealed a large number of lines. Careful analysis of the angular variations of the ENDOR spectra in the three planes perpendicular to the reference axes and recorded for several magnetic field values at each orientation yielded 13 hyperfine coupling tensors in total, all originating from proton hyperfine interactions. The tensors are listed in Table 1. The angular variations of the ENDOR lines calculated from these tensors are shown as solid lines in Supporting Information Figure S1, together with the experimental data points.

Because of the so-called Schonland ambiguity,[30] in general, two different hyperfine coupling tensors are found for each hyperfine coupling, fitting the data points of high-frequency ENDOR branches in three orthogonal planes equally well. One of them is a mathematically valid solution without physical meaning. Traditionally, this problem is solved by measuring in a fourth, skewed plane. As will be shown in a forthcoming paper from our laboratories, this ambiguity may also be solved by using both low- and high-frequency branches of a hyperfine coupling in a single crystal ENDOR experiment.[31] Neither of these techniques were applied in the current work because, in most cases, either the two tensors were (accidentally) virtually identical or one of the two tensors could be readily dismissed on account of the symmetry properties of the principal values. However, neither of these options applied to HF1(R2) and HF1(R4), and therefore, both shapes are reported in Table 1. Especially for HF1(R4), the two possible tensors are distinctly different.

A large number of EIE measurements at several orientations showed that eight of the tensors could be assigned to four radical

TABLE 1: Proton Hyperfine Coupling Tensors (in MHz) in K2G1P Single Crystals, Measured at 77 K after *in situ* X-Irradiation at This Temperature[a]

				eigenvectors		
radical	coupling	iso	aniso	*a**	*b*	*c*
R1	HF1	79.24	−3.86	0.546	−0.365	−0.754
			−3.30	0.626	0.776	0.077
			7.16	0.557	−0.514	0.653
	HF2	71.71	−4.81	0.062	0.612	−0.788
			−2.87	0.394	0.711	0.583
			7.68	0.917	−0.346	−0.197
R2	HF1a	−41.55	−22.97	0.705	−0.298	−0.643
			0.63	0.238	0.954	−0.182
			22.34	0.668	−0.024	0.744
	HF1b	−41.53	−21.45	0.744	0.134	−0.654
			−2.41	0.046	0.967	0.251
			23.86	0.666	−0.216	0.714
	HF2	15.78	−2.54	0.651	−0.754	0.087
			−1.78	0.596	0.436	−0.674
			4.31	0.471	0.491	0.733
	HF3	10.16	−3.40	0.333	−0.700	0.632
			−2.35	0.430	−0.484	−0.762
			5.75	0.839	0.525	0.140
R3	HF1	−50.97	−31.07	0.928	0.078	−0.363
			2.33	0.285	0.479	0.830
			28.75	0.239	−0.874	0.423
R4	HF1a	−61.22	−29.35	0.750	0.104	−0.653
			0.17	0.526	0.504	0.685
			29.18	0.400	−0.857	0.323
	HF1b	−61.01	−32.89	0.697	0.285	−0.658
			6.32	0.704	−0.099	0.703
			26.57	0.135	−0.953	−0.270
	HF2	24.03	−6.36	0.375	0.540	−0.753
			−3.58	0.627	0.451	0.636
			9.94	0.683	−0.711	−0.169
	HFU1	46.78	−5.61	0.423	−0.520	−0.742
			−1.52	0.741	0.670	−0.047
			7.12	0.521	−0.530	0.669
	HFU2	41.51	−4.94	0.375	−0.528	−0.762
			−3.06	0.699	0.701	−0.142
			8.00	0.609	−0.479	0.632
	HFU3	21.04	−6.77	0.066	−0.030	0.997
			−6.39	0.994	−0.082	−0.068
			13.15	0.084	0.996	0.024
	HFU4	5.82	−1.47	0.001	−1.000	0.002
			−0.64	0.284	−0.001	−0.959
			2.12	0.959	0.001	0.284
	HFU5	4.86	−1.52	0.159	−0.968	−0.194
			−0.63	0.228	0.227	−0.947
			2.15	0.961	0.107	0.257

[a] The tensors were determined by fitting the ENDOR data from angular variations in the three planes constituted by the direct crystal axes. The assignment of eight of these couplings to a total of four radical species was based on EIE measurements.

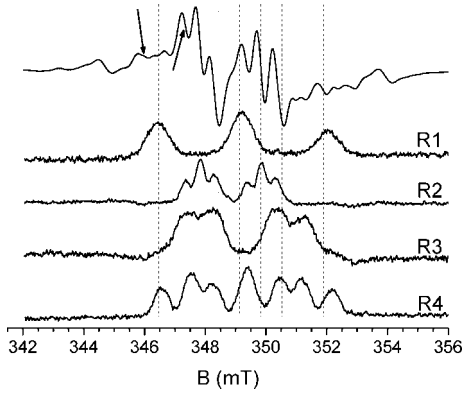

Figure 2. Top to bottom: EPR spectrum and EIE spectra of radical species R1−R4. All spectra are normalized to a microwave frequency of 9.7750 GHz. The magnetic field is oriented in the plane perpendicular to ⟨*b*⟩, approximately 10° from ⟨*a*⟩, and 10° from ⟨*a**⟩. The arrows indicate at which positions the ENDOR spectra of Figure 3 were recorded.

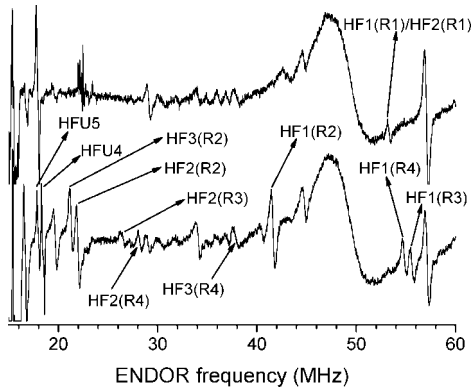

Figure 3. ENDOR spectra recorded on the EPR spectrum of Figure 2 at magnetic field values of 347.33 mT (bottom) and 345.94 mT (top). ENDOR lines are labeled according to the labeling scheme in Table 1.

species, labeled R1−R4, as indicated in Table 1. Detailed analysis of the EIE spectra at different orientations revealed that tensors HFU1−HFU3 cannot be attributed to any of those four radical species: the EIE spectra of radical species R1−R4 do not accommodate additional hyperfine couplings of the size of HFU1−HFU3, and on the few occasions where EIE spectra of some intensity were obtained on the HFU1−HFU3 ENDOR signals, they did not match those of R1−R4. The EIE spectra allowed for no conclusions concerning HFU4 and HFU5. These small hyperfine couplings would not be resolved in EIE, and the corresponding ENDOR signals are located in the very crowded region near the free proton frequency. A number of ENDOR lines could not be analyzed at all because of a very low signal-to-noise ratio at most orientations and/or because of large distortions of the ENDOR spectrum in the 45−50 MHz range as well as in the range above 60 MHz (due to technical reasons).

In the top of Figure 2, the EPR spectrum for an orientation in the plane perpendicular to ⟨*b*⟩ is shown. The ENDOR spectra obtained by probing this EPR spectrum at two different magnetic field values are shown in Figure 3. The ENDOR lines for which the corresponding hyperfine coupling tensors were determined have been labeled in Figure 3 according to the labeling scheme in Table 1. Some other lines were labeled additionally, as they will be referred to in section 4. The EIE spectra of radicals R1−R4, recorded by probing the ENDOR spectra of Figure 3, are also shown in Figure 2. Visual inspection indicates that radical species R2, which also gives rise to the most intense ENDOR lines, is by far the most abundant one. This conclusion is confirmed by similar comparisons at a number of other orientations and by simulations (section 4.5).

In addition to radicals R1−R4, the ENDOR as well as EIE spectra reveal evidence for at least three other minority radicals that unfortunately could not be analyzed in detail. ENDOR lines were obtained at some orientations, yielding EIE spectra different from those of R1−R4. Supporting Information Figures S2 and S3 show these spectra with short descriptions of their origin in the corresponding figure captions. In particular, two different radicals (designated R6 and R7 in Supporting Information Figure S3) each appear to exhibit at least two hyperfine couplings giving rise to ENDOR lines at frequencies larger than 60 MHz at most orientations and hence out of reach for the present experiments. These radicals seem to account for the more intense outer features of the EPR spectrum (see Figure 1) that cannot be attributed to radicals R1−R4. The low-frequency ENDOR lines of these couplings were observed at several orientations, but they suffered from a low signal-to-noise ratio and were generally located in a crowded frequency range, so that insufficient data could be collected to allow for hyperfine tensor determinations.

Preliminary experiments were performed with the aim of determining if the phosphoryl radicals observed in refs 13 and 14 are formed upon annealing after 77 K irradiation. Phosphoryl radical signals were indeed observed after annealing to RT. The signals are very faint at RT but become well detectable when the sample is recooled to 100 K. Due to the very low signal-to-noise ratio upon annealing, it has not been established yet at which precise temperature the formation of the phophoryl radicals takes place and which sugar radical(s) act(s) as precursor(s). This matter will be the subject of future work in our laboratories. In the next section, a detailed discussion of radical species R1−R4 will be given.

4. Discussion

4.1. Radical Species R1. Radical species R1 exhibits two typical β-proton hyperfine couplings with comparable isotropic hyperfine coupling values of approximately 72 and 79 MHz (Table 1), in agreement with the triplet structure of the EIE spectrum observed at most orientations. It is well-known that for β-proton hyperfine couplings the eigenvector associated with the most positive principal value ($b_{+,\mathrm{dip}}$) is roughly parallel with the line connecting the site of the (main) spin density with the interacting nucleus. Therefore, a comparison was made between the $b_{+,\mathrm{dip}}$ eigenvectors and the directions of the different crystallographic $C_\alpha\cdots H_\beta$ directions. Only for the C3 carbon a good agreement was found for both hyperfine couplings: the $b_{+,\mathrm{dip}}$ eigenvector directions of HF1(R1) and HF2(R1) deviate less than 20° from the crystalline C3···H2 and C3···H4 directions, respectively (Table 2). This single experimental observation leads us to propose the radical model depicted in Figure 4 (M1) where the H3 hydrogen is removed from the C3 carbon.

Assuming that the β-proton hyperfine coupling is due to hyperconjugation, the Heller−McConnell relation[32] can be applied:

$$a_{\mathrm{iso}}^{\beta} = \rho^{\pi}(B_0 + B_2 \cos^2 \theta)$$

Here, a_{iso}^{β} is the isotropic β-proton hyperfine coupling, ρ^{π} is the spin density in the lone electron orbital (LEO), and θ is the dihedral angle between the LEO and the $C_\beta-H_\beta$ bond, viewed along the $C_\alpha-C_\beta$ bond. B_0 and B_2 are empirical constants arising

TABLE 2: Comparison of Pristine Crystal Directions (Left-Hand Column) with the Eigenvectors Associated with the Most Positive Anisotropic Coupling Values of Certain Hyperfine Tensors (Top Right-Hand Side)[a]

			direction cosines			δ (deg)						
	hydrogen position	distance (Å)	*a**	*b*	*c*	HF1(R1)	HF2(R1)	HF2(R2)	HF3(R2)	HF1a(R4)	HF1b(R4)	HF2(R4)
C3···H2	β	2.08	0.355	0.758	0.548	19.2						
C3···H4	β	2.04	−0.781	0.611	0.128		17.5					
C1···H3	γ	2.73	−0.131	−0.329	−0.935			24.6				
C1···H5	γ	2.68	−0.838	−0.481	−0.260				7.3			
C3···H3	α	0.96	0.149	−0.984	−0.102					29.5	9.9	
C3···H4	β	2.04	−0.781	0.611	0.128							8.3
C4···H3	β	2.04	0.781	−0.586	−0.215							9.4
C4···H4	α	1.00	−0.138	0.987	−0.081					21.9	19.3	
C6···H5	β	2.19	0.654	−0.734	−0.182							1.8
C6···H6b	α	1.00	0.148	0.988	0.041					23.1	18.0	

[a] The labeling scheme of Table 1 is used.

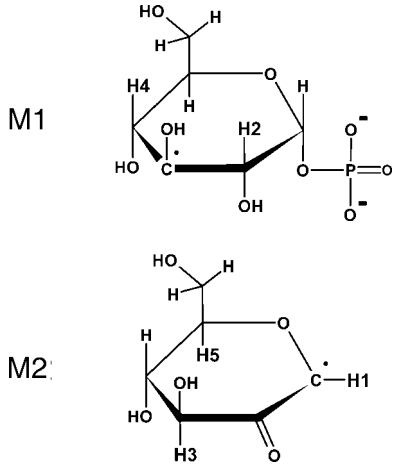

Figure 4. The chemical structures of model M1 for radical R1 and model M2 for radical R2.

from spin polarization and hyperconjugation, respectively. For a regular, planar alkyl radical, $B_0 \approx 0$ MHz and $B_2 \approx 126$ MHz can be assumed.[33] Assuming that the LEO is oriented along the original C3−H3 bond after H3 abstraction, dihedral angles of 2.8 and 10.5° are obtained for the H2 and H4 protons, respectively. Even when assuming a rather low spin density of 0.8, these dihedral angles would give rise to isotropic couplings of about 100 MHz according to the Heller−McConnell relation above, substantially larger than the experimental values of approximately 80 and 70 MHz. Moreover, the O3−HO3 bond is nearly parallel with the C3−H3 bond, and therefore, a substantial isotropic coupling of the unpaired electron with the HO3 hydroxy proton is expected for the proposed radical model. However, no ENDOR transitions that could be assigned to this interaction were observed and the recorded EIE spectra can only accommodate an additional coupling of maximum 0.5 mT (≈14 MHz).

These observations do not necessarily invalidate the proposed model (M1). A possible explanation is that the molecule undergoes some structural reorganization upon hydrogen abstraction at C3. Apart from the rather convincing match in directions (Table 2) for both β-protons, another argument favoring the proposed radical model is the positive identification of radicals at similar loci in glucose,[34−36] rhamnose,[15,37] sorbose,[38] and fructose.[39,40] These are all six-membered glucose ring carbohydrates, albeit with different molecular environments in the crystalline state.

4.2. Radical Species R2. As noted above (and as will be illustrated in section 4.5), R2 accounts for the major part of the EPR spectrum, implying that it is by far the most abundant radical species present in X-irradiated K2G1P at 77 K. This radical exhibits three appreciable hyperfine interactions. The largest coupling is due to an α-proton hyperfine interaction, as indicated by the characteristic symmetry of its anisotropic components. Both isotropic and anisotropic coupling values are substantially reduced as compared to those for "typical" α-proton hyperfine couplings, however, indicating strong delocalization of the unpaired electron. The two smaller hyperfine couplings could originate from β- as well as γ-protons.

There is a striking similarity between the tensors of R2 and those of the stable T2/T3 radical species in room temperature irradiated sucrose single crystals,[28] both for the isotropic and anisotropic components. Also, the R2 resonance exhibits a marked shift toward higher *g* values (see, e.g., the EIE spectra in Figure 2), as is the case for the T2/T3 resonance. In ref 41, T2/T3 was identified as a glucose-centered radical with the major part of the unpaired spin residing at C1, resulting from glycosidic bond cleavage at the glucose side with a concerted formation of a carbonyl group at the C2 carbon. DFT calculations showed that a substantial part of the unpaired spin is localized on both this carbonyl group and the ring oxygen, giving rise to the reduced magnitude of the α-proton hyperfine coupling, the enhanced *g*-tensor anisotropy, and the two unusually strong γ-proton hyperfine interactions.

The similarity of the experimental data of T2/T3 and R2 suggests an analogous model for R2 in K2G1P, as depicted in Figure 4 (M2). It involves scission of the sugar−phosphate linkage and thus formation of a (not paramagnetic and thus) EPR silent inorganic phosphate group. In Table 2, a comparison is made between the $b_{+,\mathrm{dip}}$ eigenvector directions of the HF2(R2) and HF3(R2) β-type tensors with the relevant directions calculated from the atomic coordinates of the K2G1P crystal structure analysis. Considering the expected delocalization of the unpaired spin density of this structure, the relatively small angular deviations (25 and 7°) support the proposed radical structure.

Additional arguments in favor of the proposed model can be obtained from the α-proton hyperfine coupling. For α-couplings, the eigenvector associated with the intermediate anisotropic coupling value ($a_{0,\mathrm{dip}}$) is oriented roughly along the LEO axis and the eigenvector associated with the most positive anisotropic coupling value ($a_{+,\mathrm{dip}}$) roughly along the $C_\alpha-H_\alpha$ bond. Upon scission of the C1−O ester bond, the C1 radical center is expected to become nearly planar, with the LEO oriented perpendicular to the plane of the glucose ring. Defining this plane as the plane formed by the C1, C3, and C5 carbons,

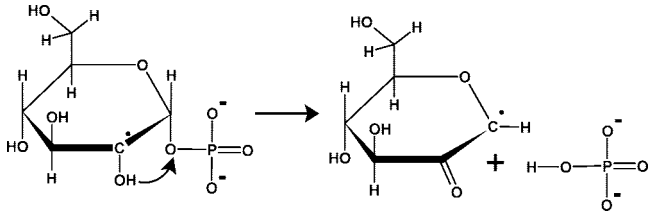

Figure 5. Possible formation mechanism of radical model R2.

angular deviations of 22 and 16° are found between the normal to the plane and the $a_{0,dip}$ eigenvectors of tensors HF1a(R2) and HF1b(R2), respectively. The H1 hydrogen atom should be oriented approximately along the bisector of the angle formed by the ring oxygen, the C1 carbon, and the C2 carbon. This direction deviates by about 34 and 25° from the $a_{+,dip}$ eigenvectors of HF1a(R2) and HF1b(R2), respectively. In conclusion, the evidence favoring model M2 proposed in Figure 4 is quite convincing and the comparison with crystal directions favors tensor HF1b(R2) over HF1a(R2).

A homolytic bond dissociation of the C1−OP ester bond automatically gives rise to a phosphoranyl-type radical in addition to a C1-centered radical. Although phosphate-centered radicals are present at RT, they have not been detected at 77 K.[13] It is therefore more probable that radical R2 is a secondary radical species originating from a hydroxyalkyl radical precursor. Starting from a C2-centered hydroxyalkyl radical, a β-phosphate elimination process[3] would directly lead to the radical structure proposed for radical R2 (M2 in Figure 4). Therefore, we suggest the formation mechanism presented in Figure 5.

4.3. Radical Species R3. At most orientations, the EIE spectrum of radical R3 is a broad doublet, arising from the α-proton hyperfine interaction reported in Table 1. At certain orientations, however, a smaller splitting, reaching up to 0.9 mT, is resolved in the EIE spectra, as demonstrated in Figure 2. Although the ENDOR signal of at least one smaller interaction was observed at some orientations, it is poorly or not resolved for most orientations and sufficient data to perform a reliable tensor analysis could not be collected. This ENDOR signal is labeled HF2(R3) and indicated in Figure 3. It could not be established whether or not this interaction is due to an exchangeable proton.

A large number of possible radical models can be envisioned if drastic geometric reorganizations such as ring opening events are considered. However, the two simplest radical models that may account for the experimental data are depicted in Figure 6: in model M3a, the sugar−phosphate linkage is broken at the glucose side, and in model M3b, a hydrogen atom at C6 is abstracted. If M3a is the correct model for R3, and assuming that the model proposed above for R2 is correct, one would expect the eigenvectors of HF1(R3) to be similar to those of HF1(R2). The data in Table 1 show that this is clearly not the case. Calculations analogous to those made above for HF1(R2) give an angle of about 60° between the $a_{0,dip}$ eigenvector of HF1(R3) and the direction perpendicular to the ring plane and an angle of about 30° between the $a_{+,dip}$ eigenvector and the bisector of the angle formed by the ring oxygen, the C1 carbon, and the C2 carbon. These values are large and suggest M3a is not a valid model.

For model M3b, the angle between the $a_{+,dip}$ eigenvector and the C_6-H_{6B} bond direction is about 26°. This indicates that the radical obtained by H6a removal may be a plausible model. However, it is hard to assess how the remaining H6b α-proton will reorient upon hydrogen abstraction and hence the small angular deviation could be fortuitous. M3b was suggested as a

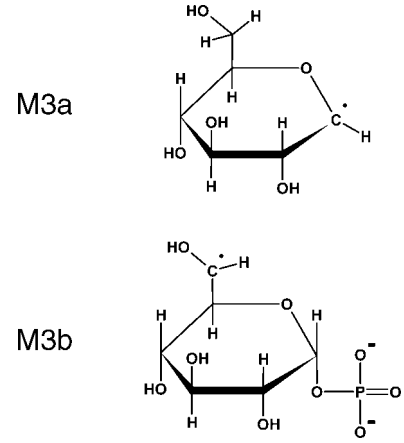

Figure 6. The chemical structure of models M3a and M3b for radical R3.

model for a radical formed and stabilized after 4 K irradiation by Locher and Box.[12] In Table 3, the three proton hyperfine coupling tensors determined by these authors are listed and compared with the R3 hyperfine coupling tensors from Table 1. The A1 tensor is quite similar to the HF1(R3) tensor in both isotropic and anisotropic hyperfine coupling values. The agreement in eigenvector directions is less good but not unreasonable considering the difference in irradiation and measurement temperatures. The A2 tensor could be accounted for by the smaller splitting observed in the EIE spectra, but the A3 hyperfine interaction originating from the HO6 hydroxy proton is not at all accommodated by the EIE spectra. Therefore, a reorientation of the hydroxy group, giving rise to a negligible isotropic component and a small anisotropic component throughout the plane perpendicular to $\langle b \rangle$ (where a number of EIE spectra were recorded), would be required for this model to be valid. Further discussions on this point are given in paper II (ref 23).

4.4. Radical Species R4. Radical R4 is characterized by three hyperfine coupling interactions, as demonstrated by the EIE spectrum shown in Figure 2, as well as by a number of EIE spectra obtained at other orientations. However, for one of the interactions (henceforth labeled HF3(R4) and indicated in Figure 3), it was not possible to obtain sufficient ENDOR data to allow for a hyperfine coupling tensor analysis, and therefore, only two hyperfine coupling tensors are presented in Table 1. HF1(R4) clearly is an α-proton hyperfine coupling. Both the isotropic (via the McConnell relation[42,33]) and the anisotropic (via the Gordy−Bernhard relation[43,44]) coupling values indicate that about 85% of the spin density is residing at the C_α carbon. HF2(R4) exhibits a typical β-proton hyperfine coupling character. The angular variation of the R4 EIE spectra in the plane perpendicular to $\langle b \rangle$, shown in Figure 7, indicates that the HF3(R4) coupling varies roughly between 1.3 and 2.2 mT in this plane, suggesting that the anisotropic part of the coupling varies at least about 25 MHz. This indicates that HF3(R4) is either an α-proton or a β-type hydroxy proton hyperfine coupling.

In Figure 8, a comparison is made between the EIE spectra obtained at nearly coincidental orientations for a nondeuterated (bottom, "H_2O spectrum") and a deuterated sample (top, "D_2O spectrum") by probing an ENDOR line of the HF1(R4) hyperfine interaction. The clear difference in spectrum shape indicates that the HF3(R4) interaction is indeed due to a hydroxy proton. The shape of the EIE spectrum for the deuterated sample can be explained only if incomplete deuteration is assumed. This point will be discussed further below.

TABLE 3: Hydrogen Hyperfine Tensors for a Hydroxyalkyl Radical Present after 4 K Irradiation of K2G1P Single Crystals, As Reported by Locher and Box[12,a]

			eigenvectors									
coupling	iso	aniso	*a**	*b*	*c*			δ (deg)				
A1	−53.12	−32.10	0.983	−0.089	0.159	HF1(R3)	32.0	HF1a(R4)	51.3	HF1b(R4)	44.7
		0.69	−0.131	0.263	0.957		28.1		44.1		86.2
		31.41	−0.127	−0.961	0.247		23.9		31.5		21.1
A2	22.28	−7.32	0.298	0.583	−0.756			HF2(R4)	5.1		
		−2.73	0.688	0.400	0.539				6.9		
		10.04	0.644	−0.708	−0.292				7.4		
A3	44.64	−13.25	0.645	−0.383	−0.662						
		−9.03	0.194	−0.755	0.627						
		22.28	0.739	0.532	0.412						

[a] On the right-hand side, eigenvector directions are compared with those of tensors determined from 77 K measurements (this study, Table 1).

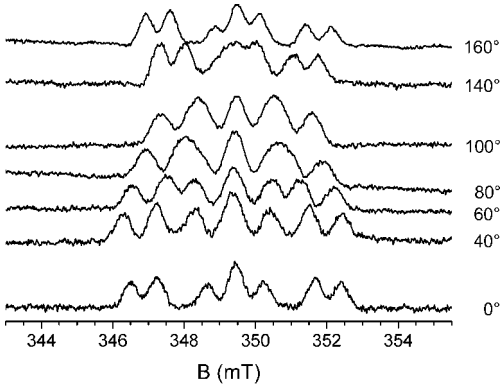

Figure 7. Angular variation of the EIE spectrum of radical R4 in the plane perpendicular to $\langle b \rangle$. The angle scale is such that $\langle a \rangle$, $\langle a^* \rangle$, $\langle c^* \rangle$, and $\langle c \rangle$ approximately correspond to 50, 70, 140, and 160°, respectively. All spectra are normalized to 9.7750 GHZ.

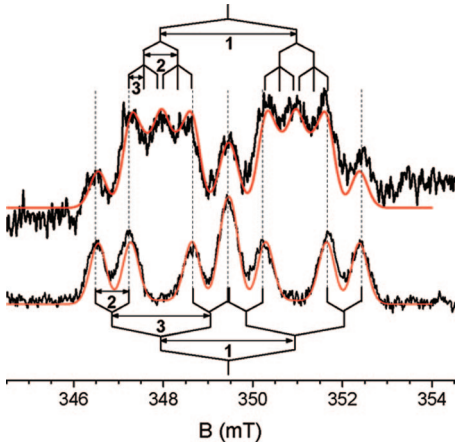

Figure 8. Experimental EIE spectrum of radical R4 in K2G1P single crystals grown from an H_2O solution (bottom, black) and from a D_2O solution (top, black). The magnetic field is oriented in the plane perpendicular to $\langle b \rangle$, approximately 20° from $\langle c \rangle$, and 40° from $\langle c^* \rangle$. The spectra are normalized to a microwave frequency of 9.7771 GHz. The numbers 1, 2, and 3 refer to hyperfine interactions HF1, HF2, and HF3, respectively. The red lines are simulations, using a line width of 0.40 mT. For other details concerning the simulation (parameters), we refer to the text.

The presence of an α-proton hyperfine coupling again severely limits the number of reasonably simple radical models, as it did for radical species R3. For R4, however, the information offered by the β-proton, which in general is expected to undergo less geometric reorganization as compared to an α-proton, can be used. As shown in Table 2, there are three $C_\alpha \cdots H_\beta$ directions that deviate less than 10° from the $b_{+,\mathrm{dip}}$ eigenvector direction

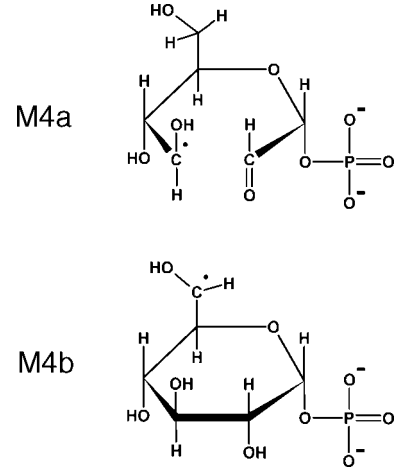

Figure 9. The chemical structure of models M4a and M4b for radical R4. Model M4b is the same as model M3b (Figure 6).

of HF2(R4), yielding C3, C4, and C5 as possible radical centers. For all three possibilities, an α-proton is present such that the $C_\alpha - H_\alpha$ is directed roughly along the $a_{+,\mathrm{dip}}$ eigenvector of HF1(R4) (Table 2). The additional requirement of the presence of a β-type hydroxy proton then yields the two possible models depicted in Figure 9. Model M4a could be formed through spontaneous electronic reorganization from the O2-centered alkoxy radical, present at 4 K (see the Introduction). As model M4a has a broken ring structure, substantial geometric changes may occur and further analysis through comparison with pristine crystal directions is not warranted. Model M4b is the hydroxyalkyl radical suggested to be present at 4 K by Locher and Box[12] (Table 3), which was also found to be a possible model for radical R3 (model M3b). The A2 hyperfine coupling tensor is in good agreement with HF2(R4), both in principal values and eigenvector directions. This already strongly suggests that the R4 radical is very similar to the species detected at 4 K. Hyperfine tensors A1 and HF1(R4) are similar but show larger discrepancies. Again, such differences may be due to the differences in irradiation and measuring temperatures, which may lead to slight geometric differences in the radical structure. The anisotropy in the rot $\langle b \rangle$ plane predicted by the A3 tensor amounts to about 26 MHz, in very good agreement with the findings from the EIE angular variations and the isotropic component of A3 is also reconcilable with the findings from the EIE spectra. Nevertheless, the EIE angular variation of Figure 7 is reproduced poorly when the A3 tensor as reported by Locher and Box[12] (Table 3) is employed (Supporting Information Figure S4). However, there is a Schonland ambiguity (see above and refs 30 and 31) for the A3 tensor, and

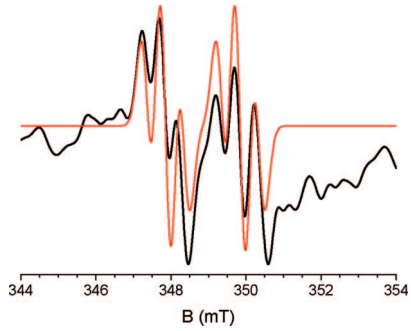

Figure 10. Experimental EPR spectrum of Figure 2 (black) and simulated EPR spectrum of radical R2 (red), using the hyperfine tensors listed in Table 1 and a line width of 0.40 mT. The spectra are normalized to a microwave frequency of 9.7750 GHz.

therefore, the seven other tensors, obtained by varying the sign of the off-diagonal elements of A3 in the reference frame, should also be considered. The EIE angular variation is in fact reproduced quite well when employing the tensor obtained by changing the signs of $A3_{12}$ (=$A3_{21}$) and $A3_{13}$ (=$A3_{31}$) tensor elements in the reference frame, as illustrated in Supporting Information Figure S4. As these changes of sign correspond to performing an $a \rightarrow -a$ operation on the principal directions, while leaving the principal values of A3 unaltered, this tensor is denoted A3[$-a$]. In paper II (ref 23), DFT calculations provide additional convincing arguments that A3[$-a$] is the correct tensor shape.

To interpret the spectrum shape of the "D_2O spectrum" in Figure 8, the "H_2O spectrum" was first reproduced as accurately as possible. Since HF1(R4) and HF2(R4) were determined in the present experiments, only adjustments of the A3[$-a$] coupling are justifiable. The best agreement (Figure 8, bottom red line) is found when an effective coupling size of 60 MHz is assumed for A3, which is about 9 MHz larger than the value the A3[$-a$] tensor yields for this orientation (and 25 MHz larger than the "original" A3 tensor yields). Using these parameters, the "D_2O spectrum" can be reproduced quite satisfactorily if a deuteration rate of about 60% is assumed (Figure 8, top red line). This is about 30% lower than may be expected (cf. section 2), which could be due to either differences in relaxation rates between the radical species in the deuterated and the nondeuterated crystal or an isotope effect on the radical formation of species R4.

4.5. Relative Abundance of the Different Radical Species. The EIE spectra of radicals R1−R3 in Figure 2 can be accurately reproduced using the tensors in Table 1, treating the g values and linewidths as variables. As illustrated above, also for R4, the EIE spectrum can be reproduced satisfactorily at this orientation when increasing the isotropic component of A3 by 9 MHz. Using these parameters to simulate the (composite) EPR spectrum, an indication of the relative abundances of the different radical species can be obtained. Figure 10 shows the experimental EPR spectrum of Figure 2, together with a simulation of the R2 EPR spectrum, using a line width of 0.40 mT. The agreement is good, but apart from the complete absence of the outer features of the EPR spectrum in the simulation, there are also some minor discrepancies in the central part. Manually mixing in various small concentrations of R1, R3, and R4 did not noticeably improve the fitting. In fact, simulations indicate that even a relative abundance of 5% for any of these species would give rise to features not observed in the EPR spectrum. As no reliable lower limit can be given, we merely conclude that these species are far less abundant than R2. The major part of the remaining discrepancies should therefore be attributed to one or more other radical species, most probably those also giving rise to the outer EPR signals (R6 and R7, see above and the Supporting Information).

5. Conclusions

At least seven different carbon-centered radical species are formed in K2G1P single crystals upon irradiation at 77 K. The dominant radical is identified as a C1-centered species, formed by a net scission of the glucose−phosphate bond and concerted formation of a carbonyl group at C2. Two of the minority radicals are most likely C3- and C6-centered, formed by net hydrogen abstractions at these positions, but some uncertainty about these interpretations from the experimental data alone remains. It could not be determined in the current work which radical species acts as a precursor for the phophoryl radicals observed at 280 K. In paper II (ref 23), DFT calculations confirm the validity of the proposed radical structures and provide insight in their precise conformation and possible formation mechanisms in addition to providing elementary insight into the radiation chemistry of sugars.

Acknowledgment. The authors H.D.C. (Research Assistant) and E.P. (Postdoctoral Fellow) wish to thank the Fund for Scientific Research - Flanders (FWO) for financial support. The European Cooperation in the field of Scientific and Technical Research (COST action p15) is also acknowledged for financial support.

Supporting Information Available: Coordinates of 35 atoms in K2G1P single crystals, as reported by Sugawara and Iwasaki.[24] X-band angular variation of the ENDOR transitions in K2G1P single crystals measured at 77 K after *in situ* X-irradiation at this temperature for all hyperfine interactions listed in Table 1. EIE spectra of three other radicals (R5, R6, and R7) at the orientation of Figure 2. ENDOR spectra of Figure 3, where some ENDOR lines have been labeled additionally and are assigned to radicals R5−R7. Angular variation of the EIE spectrum of radical R4 in the plane perpendicular to ⟨b⟩ (same as Figure 7) and simulation of these spectra using tensors HF1(R4) and HF2(R4) (Table 1) and tensor A3 (Table 3) or tensor A3[$-a$] (see section 4.4 for details). This material is available free of charge via the Internet at http://pubs.acs.org.

References and Notes

(1) Bernhard, W. A.; Close, D. M. In *DNA Damage Dictates the BiologicalConsequences of Ionizing Irradiation: The Chemical Pathways In Charged Particle and Photon Interactions with Matter: Chemical, Physicochemical, and Biological Consequences with Applications*; Mozumber, A., Hatano, Y., Eds.; Marcel Dekker: New York, 2003; pp 431−470.

(2) Becker, D.; Adhikary, A.; Sevilla, M. D. In *The Role of Charge and Spin Migration in DNA Radiation Damage In Charge Migration in DNA Physics, Chemistry and Biology Perspectives*; Chakraborty, T.; Springer-Verlag: Berlin, Heidelberg, 2007; pp 139−175.

(3) von Sonntag, C. *The Chemical Basis of Radiation Biology*; Taylor and Francis: London, 1987.

(4) Boudaïffa, B.; Cloutier, P.; Hunting, D.; Huels, M. A.; Sanche, L. *Science* **2000**, *287*, 1658–1660.

(5) Simons, J. *Adv. Chem. Res.* **2006**, *39*, 772–779.

(6) Kumar, A.; Sevilla, M. D. In *Radiation Induced Molecular Phenomena in Nucleic Acids: A Comprehensive Theoretical and Experimental Analysis*; Shukla, M. K., Leszczynski, J.; Springer-Verlag: Berlin, Heidelberg, New York, 2008.

(7) Becker, D.; Bryant-Friedrich, A.; Trzasko, C.; Sevilla, M. D. *Radiat. Res.* **2003**, *160*, 174–185.

(8) Ezra, F. S.; Bernhard, W. A. *J. Chem. Phys.* **1973**, *59*, 3543–3549.

(9) Fouse, G. W.; Bernhard, W. A. *J. Chem. Phys.* **1979**, *70*, 1667–1670.

(10) Baine, T. J.; Sagstuen, E. *Radiat. Res.* **1998**, *150*, 148–158.

(11) Nelson, D.; Symons, M. C. R. *J. Chem. Soc., Perkin Trans. 2* **1977**, 286–293.

(12) Locher, S. E.; Box, H. C. *J. Chem. Phys.* **1980**, *72*, 828–832.

(13) Sanderud, A.; Sagstuen, E. *J. Chem. Soc., Faraday Trans.* **1996**, *92*, 995–999.

(14) Bungum, B.; Hole, E. O.; Sagstuen, E.; Lindgren, M. *Radiat. Res.* **1994**, *193*, 194–202.

(15) Sagstuen, E.; Lindgren, M.; Lund, A. *Radiat. Res.* **1991**, *128*, 235–242.

(16) Madden, K. P.; Bernhard, W. A. *J. Phys. Chem.* **1980**, *84*, 1712–1717.

(17) Becker, D.; Bryant-Friedrich, A.; Trzasko, C.; Sevilla, M. D. *Radiat. Res.* **2003**, *160*, 174–185.

(18) Beevers, C. A.; Maconochie, G. H. *Acta Crystallogr.* **1965**, *18*, 232–236.

(19) Narendra, N.; Viswamitra, M. A. *Curr. Sci.* **1984**, *53*, 1018–1020.

(20) Bungum, B. MSc Thesis, Dept. Physics, University of Oslo, 1993.

(21) Nelson, D. J.; Symons, M. C. R.; Wyatt, J. L. *J. Chem. Soc., Faraday Trans.* **1993**, *89*, 1955–1958.

(22) The authors of ref 21 mistakenly reported these results to be obtained on the disodium salt. A correction was made in ref 13.

(23) Pauwels, E.; De Cooman, H.; Vanhaelewyn, G.; Sagstuen, E.; Callens, F.; Waroquier, M. *J. Phys. Chem B* **2008**, *112*, 15054−15063.

(24) Sugawara, Y.; Iwasaki, H. *Acta Crystallogr.* **1984**, *C40*, 389–393.

(25) Ohman, K. T.; Sanderud, A.; Hole, E. I.; Sagstuen, E. *J. Phys. Chem. A* **2006**, *110*, 9585–9596.

(26) Nelson, W. H. *J. Magn. Reson.* **1980**, *38*, 71–78.

(27) Sørnes, A. R.; Sagstuen, E.; Lund, A. *J. Phys. Chem.* **1995**, *99*, 16867–16876.

(28) De Cooman, H.; Pauwels, E.; Vrielinck, H.; Dimitrova, A.; Yordanov, N.; Sagstuen, E.; Waroquier, M.; Callens, F. *Spectrochim. Acta, Part A* **2008**, *69*, 1372–1383.

(29) Stoll, S.; Schweiger, A. *J. Magn. Reson.* **2006**, *178* (1), 42–55.

(30) Schonland, D. S. *Proc. Phys. Soc. London* **1959**, *73* (473), 788–792.

(31) Vrielinck, H.; De Cooman, H.; Tarpan, M. A.; Sagstuen, E.; Waroquier, M.; Callens, F. *J. Magn. Reson.*, doi: 10.1016/j.jmr.2008.09.017.

(32) Heller, C.; McConnell, H. M. *J. Chem. Phys.* **1960**, *32*, 1535.

(33) Bernhard, W. A. *Adv. Radiat. Biol.* **1981**, *9*, 199.

(34) Madden, K. P.; Bernhard, W. A. *J. Phys. Chem.* **1979**, *83* (20), 2643.

(35) Pauwels, E.; Van Speybroeck, V.; Callens, F.; Waroquier, M. *Int. J. Quantum Chem.* **2004**, *99* (2), 102–108.

(36) Pauwels, E.; Van Speybroeck, V.; Waroquier, M. *Spectrochim. Acta, Part A* **2006**, *63* (4), 795–801.

(37) Pauwels, E.; Van Speybroeck, V.; Waroquier, M. *J. Phys. Chem. A* **2006**, *110* (20), 6504–6513.

(38) Vanhaelewyn, G.; Jansen, B.; Pauwels, E.; Sagstuen, E.; Waroquier, M.; Callens, F. *J. Phys. Chem. A* **2004**, *108* (16), 3308–3314.

(39) Vanhaelewyn, G.C.A.M.; Pauwels, E.; Callens, F. J.; Waroquier, M.; Sagstuen, E.; Matthys, P. F. A. E. *J. Phys. Chem.* **2006**, *110* (6), 2147.

(40) Tarpan, M.; Sagstuen, E.; Pauwels, E.; Vrielinck, H.; Waroquier, M.; Callens, F. *J. Phys. Chem. A* **2008**, *112*, 3898.

(41) De Cooman, H.; Pauwels, E.; Vrielinck, H.; Sagstuen, E.; Callens, F.; Waroquier, M. *J. Phys. Chem. B* **2008**, *112*, 7298–7307.

(42) McConnell, H. M.; Chesnut, D. B. *J. Chem. Phys.* **1958**, *28*, 107–117.

(43) Erling, P. A.; Nelson, W. H. *J. Phys. Chem. A* **2004**, *108*, 7591–7595.

(44) Bernhard, W. A. *J. Chem. Phys.* **1984**, *81*, 5928–5935.

JP804290E